# NUMERICAL SIMULATION OF 2D FLUID FLOW USING THE FINITE ELEMENT DISCRETIZATION ON UNSTRUCTURED GRID COMBINED WITH ADAPTIVE MESH REFINEMENT TECHNIQUE

## MÔ PHỎNG SỐ DÒNG CHẢY TRONG KHÔNG GIAN HAI CHIỀU BẰNG RỜI RẠC PHẦN TỬ HỮU HẠN TRÊN LƯỚI KHÔNG CẤU TRÚC KẾT HỢP VỚI KỸ THUẬT LÀM MỊN LƯỚI CỤC BỘ

**Nguyen Manh Hung[1], Ha Truong Sang[1,*], Le Van Duong[2]**

**ABSTRACT**

The finite element method (FEM) has been successful in simulating complex physical systems in science and engineering. A big challenge of using the FEM is how to reduce computation time in large-scale problems. In this paper, we propose combining the FEM and an Adaptive Mesh Refinement (AMR) technique for solving an incompressible fluid flow on unstructured grids. We use the magnitude of the vorticity field as an indicator function to detect the region that needs to be refined and then refine the original mesh using an element subdivision technique. The governing equations are discretized using a finite element method based on the linear, equal order P1P1 elements (linear order for both velocity and pressure). The Navier-Stokes equations for unsteady fluid flow are solved using a three-step projection method with the Crank-Nicolson scheme employed for the temporal discretization of diffusion term and the Adams-Bashforth scheme for convection term. The performance of the present method is verified for several benchmark problems in 2D domains. It shows that the proposed method can provide enough accuracy compared to the previous results. Moreover, the present method can significantly reduce the CPU time compared to the traditional method without using the AMR technique.

***Keywords:*** *Adaptive mesh refinement, finite element method, unstructured mesh, incompressible flow.*

**TÓM TẮT**

Phương pháp phần tử hữu hạn đã khá thành công trong việc mô phỏng các vấn đề vật lý phức tạp trong khoa học và kỹ thuật. Một thử thách rất lớn trong việc sử dụng phương pháp phần tử hữu hạn là tối ưu thời gian tính trong những bài toán lớn. Trong bài báo này, chúng tôi trình bày sự kết hợp của phương pháp phần tử hữu hạn với kỹ thuật làm mịn lưới cục bộ để mô phỏng dòng không nén trên lưới không cấu trúc. Phương pháp này sử dụng độ lớn của vector xoáy là hàm điều khiển để xác định vùng cần làm mịn lưới, sau đó quá trình làm mịn được thực hiện thông qua việc chia nhỏ các phần tử ban đầu. Các phương trình chủ đạo được rời rạc bằng phương pháp phần tử tuyến tính không cấu trúc (tuyến tính cho cả vận tốc và áp suất). Dùng phương pháp tách ba bước kết hợp với phương pháp Crank-Nicolson áp dụng cho sự rời rạc thành phần lực nhớt và phương pháp Adams-Bashforth áp dụng cho thành phần lực quán tính để giải phương trình Navier-Stokes cho dòng không nén được. Sự hiệu quả của phương pháp này được kiểm chứng qua một số ví dụ trên miền tính toán hai chiều. Kết quả cho thấy phương pháp nghiên cứu có thể cung cấp độ chính xác cần thiết so với các kết quả đã công bố trước đó. Hơn nữa, với kỹ thuật làm mịn lưới cục bộ, phương pháp có thể giảm đáng kể thời gian tính toán so với việc không sử dụng kỹ thuật này.

***Từ khóa:*** *Làm mịn lưới cục bộ, phương pháp phần tử hữu hạn, lưới phi cấu trúc, dòng không nén.*

[1]Faculty of Mechanical Engineering, Le Quy Don Technical University
[2]Faculty of Vehicle and Energy Engineering, Le Quy Don Technical University
[*]Email: sanght.st@lqdtu.edu.vn
Received: 10/9/2021
Revised: 17/10/2021
Accepted: 15/11/2021

## 1. INTRODUCTION

During the last few decades, many numerical methods have been developed to solve the Navier-Stokes equations. The equations for unsteady fluid flow can be solved by a segregated algorithm (also called the fractional step) which obtains the pressure and velocity components separately, or by a coupled algorithm that obtains all the variables simultaneously. The former approach uses a smaller computational memory, which helps the large-scale problem, while the latter method has the advantage of convergence robustness.

The finite element method (FEM) successfully simulates complex physical problems in science and technology among the numerical approaches to solve the Navier-Stokes equations. However, a big challenge of using the FEM method is the very high computational cost, especially for the large-scale problem. Several techniques are adopted to reduce the simulation's computational time using the FEM method, such as the parallel computation, the multigrid method (MG), or the adaptive mesh refinement (AMR) technique.

To obtain an accurate solution at a lower computational work, the AMR techniques are usually used in many technology and engineering fields. For the dynamic fluid flow simulations, many problems can be treated advantageously using the AMR technique (e.g. [1, 2]). AMR techniques can be combined with the MG solver for more efficient performance, especially for simulating unsteady flows. There exist many studies on adaptive, e.g. multigrid, in literature. The steady solution is obtained using the combination of the multigrid and an adaptive algorithm based on a posteriori error estimation [3]. In their work, the mesh is initial as a coarse-grid, and the local hierarchical essential adaption is used at the high error region to get the more advanced level. The solution is obtained on the most refined grid, which is satisfied with the error criterion. This combination can be used in uniform mesh [4]. Their simulations are successful on the Cartesian grid. The uniform grid is initialized, and the local refinement technique based on the element subdivision is used to get a higher mesh resolution. In the present study, we concentrate on the unstructured grid, which is a distinguishing feature of the finite element method. The AMR technique using the vorticity magnitude of fluid flow as an indicator is investigated in the present research.

The remainder of the paper is organized as follows: Section 2, we describe the numerical method for the finite element method for incompressible Navier-Stokes flow and the AMR technique; Section 3 shows the numerical results of 2D benchmark problems for validation and discussion; Finally, some conclusions are drawn in Section 4.

## 2. NUMERIAL METHODS

### 2.1. Finite element method for incompressible flow

#### *2.1.1. Governing equations*

The fluid domain is denoted by $\Omega$ with boundary $\Gamma$. The governing equations of fluid flows are the incompressible Navier-Stokes equations which can be written as follows [5]:

$$\begin{aligned} &\nabla\cdot\mathbf{v}=0 \quad \text{in } \Omega \\ &\rho\left[\frac{\partial\mathbf{v}}{\partial t}+\mathbf{v}\cdot\nabla\mathbf{v}\right]=\nabla\cdot\sigma+\rho\mathbf{b} \quad \text{in } \Omega \end{aligned} \tag{1}$$

where $\rho$, $\mathbf{v}$, $\mathbf{b}$ and $\boldsymbol{\sigma}$ denote the fluid density, the velocity vector, the body force vector, and the stress tensor, respectively. The fluid is assumed Newtonian with the corresponding constitutive equation is written by:

$$\begin{aligned} &\boldsymbol{\sigma}=-p\mathbf{I}+\tau, \\ &\boldsymbol{\tau}=\mu[\nabla\mathbf{v}+(\nabla\mathbf{v})^T] \end{aligned} \tag{2}$$

where p, $\mu$, $\boldsymbol{\tau}$, $\mathbf{I}$ and T indicate the pressure, the fluid dynamic viscosity, the shear stress tensor, the second-order identity tensor, and the transposition, respectively. The Dirichlet and Neumann boundary conditions are described as follows:

$$\begin{aligned} &\mathbf{v}=\bar{\mathbf{v}} \quad \text{on } \Gamma_v, \\ &\boldsymbol{\sigma}\times\mathbf{n}=\bar{\mathbf{t}} \quad \text{on } \Gamma_t \end{aligned} \tag{3}$$

where **n** denotes the outward unit normal vector of the fluid boundary, and $\Gamma_\mathbf{v}$ and $\Gamma_\mathbf{t}$ - the boundaries on which the velocity $(\bar{\mathbf{v}})$ and traction $(\bar{\mathbf{t}})$ are defined, respectively.

#### *2.1.2. Fractional method*

In this study, we employ the fractional method [6] to solve the incompressible Navier-Stokes equations. The second-order-implicit Crank-Nicolson scheme is employed for the temporal discretization of the diffusion terms and the second-order-explicit Adams-Bashforth scheme for the convective terms. A fractional three-step scheme can be written as:

$$\frac{\hat{u}_i-u_i^n}{\Delta t}+\frac{1}{2}\left(3u_j^n u_{i,j}^n-u_j^{n-1}u_{i,j}^{n-1}\right)=\frac{\mu}{2\rho}\left(\hat{u}_{i,jj}+u_{i,jj}^n\right) \tag{4}$$

$$p_{,jj}^{n+1}=\frac{\rho}{\Delta t}\hat{u}_{i,i} \tag{5}$$

$$\frac{u_i^{n+1}-\hat{u}_i}{\Delta t}=-\frac{1}{\rho}p_{,i}^{n+1} \tag{6}$$

where $\Delta t$ is the time step; the superscript n denotes the time level. In this procedure, the intermediate velocity $\hat{u}$ is solved by the momentum equation (4). At the next step, the pressure is obtained by solving the Poisson equation (5), and then the velocity is corrected by the pressure (6).

#### *2.1.3. P1P1 finite element formulation*

We use the P1P1 finite element (linear order for both velocity and pressure) for all variables; the pressure is placed at the same node as the velocity. The momentum equations are discretized using a consistent streamline upwind Petrov-Galerkin method and the pressure equation using a Galerkin method, and their weak formulation can be written as follows:

Find $u\in H^1(\Omega)$, $\hat{u}\in H^1(\Omega)$ and $p\in H^1(\Omega)$ such that:

$$\begin{aligned} &\int_\Omega w_i\frac{\hat{u}_i-u_i^n}{\Delta t}d\Omega+\frac{\mu}{2\rho}\int_\Omega w_{i,j}\hat{u}_{i,j}d\Omega \\ &=\frac{\mu}{\rho}\int_{\Gamma_t} w_i\bar{t}_i^u d\Gamma-\frac{\mu}{2\rho}\int_\Omega w_{i,j}u_{i,j}^n d\Omega \\ &-\frac{1}{2}\int_\Omega w_i\left(3u_j^n u_{i,j}^n-u_j^{n-1}u_{i,j}^{n-1}\right)d\Omega \end{aligned} \tag{7}$$

$$\int_\Omega q_{,j}p_{,j}^{n+1}d\Omega=\int_{\Gamma_t} qp_{,j}^{n+1}n_j d\Gamma-\frac{\rho}{\Delta t}\int_\Omega q\hat{u}_{i,i}d\Omega \tag{8}$$

$$\int_\Omega w_i\frac{u_i^{n+1}-\hat{u}_i}{\Delta t}d\Omega=-\frac{1}{\rho}\int_\Omega w_i p_{,i}^{n+1}d\Omega \tag{9}$$

for all admissible functions $w\in V, q\in P$ where $V=\left\{w\middle|w\in H^1(\Omega), w=0 \text{ on } \Gamma_v\right\}$, $P=\left\{q\middle|q\in H^1(\Omega), q=0 \text{ on } \Gamma_p\right\}$ and $H^1(\Omega)$ denotes the Sobolev space defined on the spatial domain $\Omega$. In equation (7), $\bar{t}_i^u=u_{i,j}n_j$ denotes the Neumann boundary of velocity. It should be noted that equation (8) is the Poison-type equation.

## 2.2. Adaptive refinement mesh technique

### *2.2.1. Grid refinement indicator*

A new mesh is obtained from the primary grid by local refinement at the regions controlled by the refinement indicator. Depending on the specific problems, the indicators will be selected so that the solution on the newly obtained mesh will be sufficiently accurate with the smallest number of grid elements. It is the interface position in the two-flow problems [7]; in the unsteady fluid flow, the indicator can be chosen as an element Reynolds number [8] or the magnitude of the vorticity field [9]. The magnitude vorticity is calculated on each element using the gradient of the velocity field. For the linear tetrahedral element (four-nodes), the velocity gradient can be obtained by an analysis formula based on the velocity and the position of nodes.

In 2D computational domain, the magnitude of vorticity field is calculated by:

$$\|\boldsymbol{\omega}\| = \left\| \frac{\partial v}{\partial x} - \frac{\partial u}{\partial y} \right\| \tag{10}$$

where u and v are the vector components and can be written using the finite element approximation as follows:

$$\begin{aligned} u &= N_1u_1 + N_2u_2 + N_3u_3 \\ v &= N_1v_1 + N_2v_2 + N_3v_3 \end{aligned} \tag{11}$$

and

$$\begin{aligned} \frac{\partial u}{\partial y} &= \frac{\partial N_1}{\partial y}u_1 + \frac{\partial N_2}{\partial y}u_2 + \frac{\partial N_3}{\partial y}u_3 \\ \frac{\partial v}{\partial x} &= \frac{\partial N_1}{\partial x}v_1 + \frac{\partial N_2}{\partial x}v_2 + \frac{\partial N_3}{\partial x}v_3 \end{aligned} \tag{12}$$

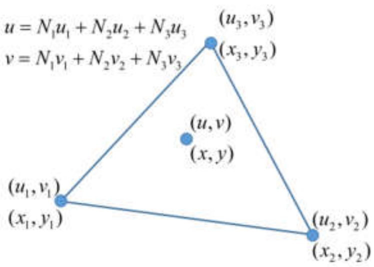


Figure 1. Linear approximation of velocity on triangle element

The $N_1$, $N_2$ and $N_3$ on the equation (11, 12) are shape-functions associated with nodes 1, 2 and node 3 on Fig. 1, respectively. The shape-function on the triangle element (Fig. 1) is the linear order of coordinate x, y. It leads to the results that the gradient of the velocity field ($\partial v/\partial x$, $\partial u/\partial y$) can be calculated using coordinate of nodes on the element. The derivative of the shape-functions on equation (12) is written detailed as follows:

$$\begin{aligned} &\frac{\partial N_1}{\partial y} = \frac{1}{J}(b-a); \quad \frac{\partial N_2}{\partial y} = \frac{-1}{J}b; \quad \frac{\partial N_3}{\partial y} = \frac{1}{J}a \\ &\frac{\partial N_1}{\partial x} = \frac{1}{J}(c-d); \quad \frac{\partial N_2}{\partial x} = \frac{1}{J}d; \quad \frac{\partial N_3}{\partial x} = \frac{-1}{J}c \end{aligned} \tag{13}$$

where $a = x_2 - x_1$, $b = x_3 - x_1$, $c = y_2 - y_1$, $d = y_3 - y_1$ and $J = ad - bc$.

Using the formula (12) and (13), the magnitude of the element in equation (10) can be directly calculated using the coordinate and the velocity of nodes on the element.

### *2.2.2. AMR based on element subdivision*

The goal of the AMR procedure is to produce a sufficient mesh resolution at the region of interest. The refinement indicator is calculated over time, and the mesh is updated continuously to ensure that the mesh resolution in the high vorticity region is always satisfactory enough. Several subdivision patterns have been proposed for unstructured meshes, such as the longest edge refinement technique, the successive bisection technique, the newest vertex bisection algorithm, or the classical techniques (h-refinement).

In this work, we adopt the classical h-refinement technique, which subdivides a triangular element into four smaller ones (1:4 subdivision) in a 2D space and a tetrahedral element - eight smaller ones (1:8 subdivision) in a 3D space. From an initially fixed grid, the adaptive zone is identified. It contains the cut element (purple elements), which has a high vorticity magnitude, the adjacent element of this cut element, and the hanging elements, shown in Fig. 2. The neighbouring element (blue elements) can be selected from one or more neighbour layers of the cut element to smooth the grid between the refined and unrefined regions. The identification process can be repeated for a higher level of refinement based on the presently refined mesh, shown in Fig. 3.

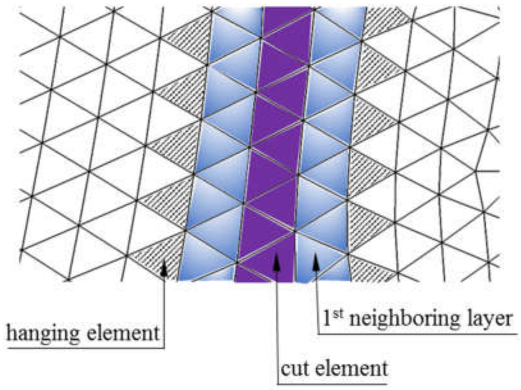


Figure 2. The initial mesh and an adaptive zone [7]

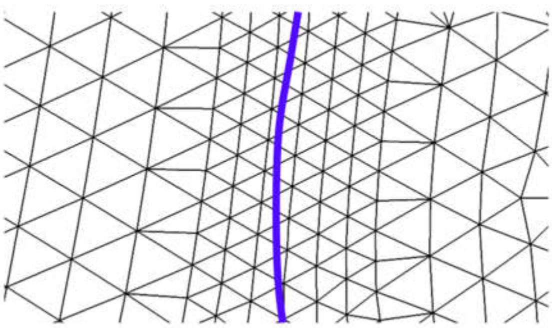

a)

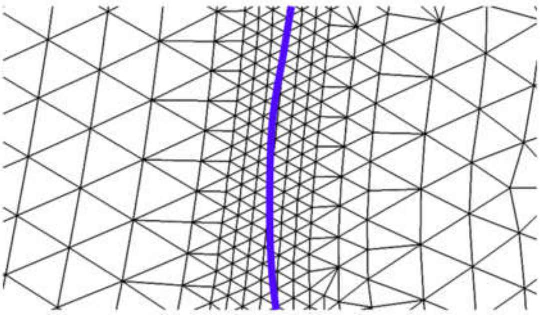

b)

Figure 3. The classical subdivision in triangular elements [7]:

a) one-level adapted mesh; b) two-level adapted mesh

In order to avoid the badly deformed elements in the final refined mesh, the higher adaptive zone of refinement can only be created at the region where the elements were subdivided regularly in the lower level of refinement. In the reference [7], the AMR technique was described in more detail and successfully validated many unsteady flow problems.

## 3. RESULTS AND DISCUSSIONS

### 3.1. Lid-driven cavity

The first benchmark is the lid-driven cavity problem; the computation domain and the boundary conditions are shown in Fig. 4. The Reynolds number is defined by Re = ρUL/μ where ρ and μ are density and viscosity, respectively. The problem is examined with Re = 100, Re = 1000, and Re = 5000.

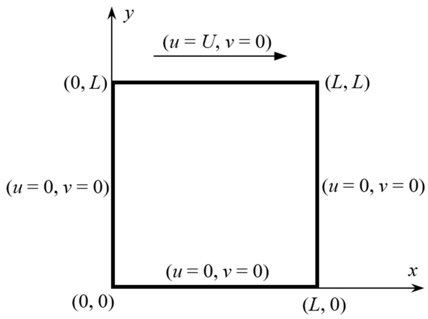


Figure 4. Schematic and boundary conditions of the 2D lid-driven cavity problem

The fractional three-step is used to solve the incompressible fluid; the AMR procedure is performed every five-time steps Δt = $5.10^{-2}$s. The CG-ILU(0) [10] method is adopted to solve the momentum and the correction velocity equations. The Poisson pressure equation is solved by using the multigrid method [11]. The basic grid and the fine grid obtained using the second level of the full refinement technique are shown in Fig. 5a and Fig. 5b, respectively. The numbers of nodes and elements of different types of the grid are listed in Table 1. It can be noted that the number of elements is increased four times after each full AMR refinement. Fig. 6 shows the streamlines of steady-state (Fig. 6a) and the comparison of vertical velocity at centerline (y/L = 0.5) for the case of Re = 1000 (Fig. 6b). It is shown that the solution of the AMR technique is in good agreement with the fine grid obtained by using the full refinement subdivision, whereas the solution in the basic grid has a significant error.

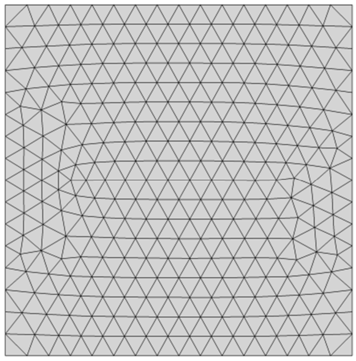

a)

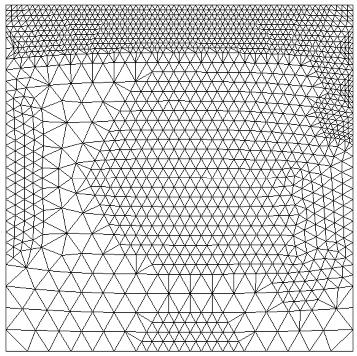

b)

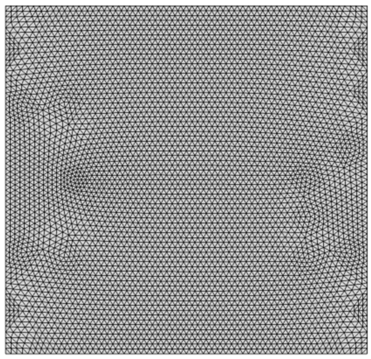

c)

Figure 5. The grid: a) Basic; b) AMR technique; c) Second full refinement subdivision

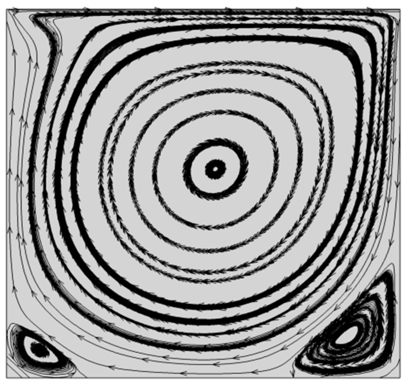

a)

P-ISSN 1859-3585 | E-ISSN 2615-9619

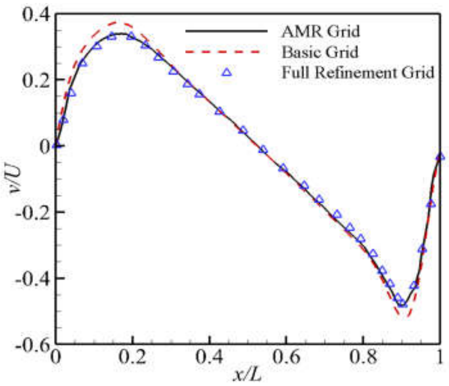


b)

Figure 6. Re =1000: a) Streamlines; b) Comparison of vertical velocity (v) at y/L = 0.5 of local AMR, basic grid and full AMR grid

Table 1. Grid information

| Type of grids | Basic | First full refinement subdivision | Second full refinement subdivision | AMR technique |
|---|---|---|---|---|
| No. nodes | 316 | 1,213 | 4,657 | 1,513 |
| No. elements | 566 | 2,264 | 9,056 | 2,866 |

Fig. 7 shows the final mesh and the vorticity contour at various Reynolds numbers. The solution is obtained at a steady state. The mesh is refined at the high magnitude vorticity to get an accurate solution. In this case, we used only one AMR level to get a final grid. The AMR-FEM code is validated by comparing velocity at the centerlines of the domain in x-direction and y-direction. The results are in good agreement with those proposed by Ghia [12], as shown in Fig. 8. Further, the computational time with AMR grid is smaller, around three times compared to that of a fine mesh using second full refinement subdivision.

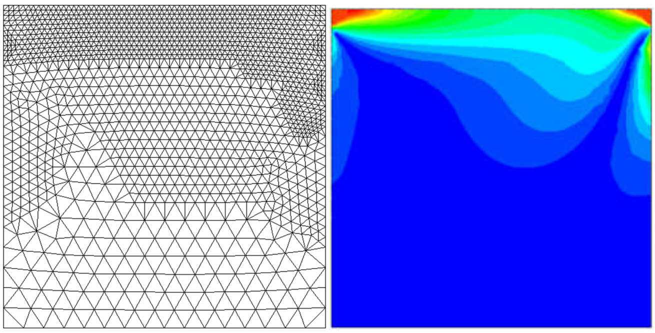

Re = 100

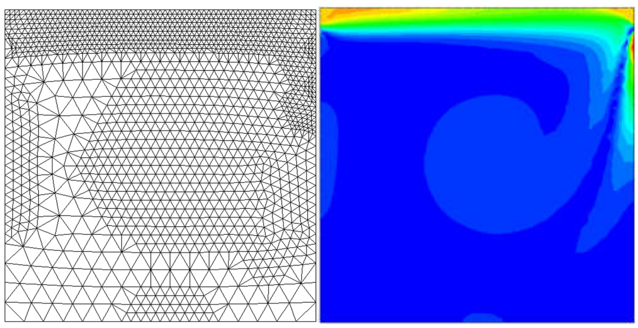

Re = 1000

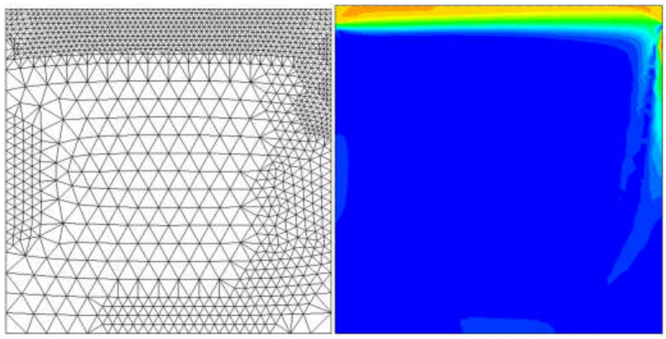

Re = 5000

Figure 7. The vorticity magnitude contour and its corresponding final mesh for various Re numbers

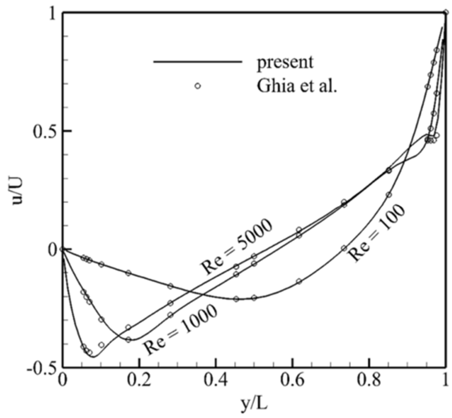


a) u-component velocity at x/L = 0.5

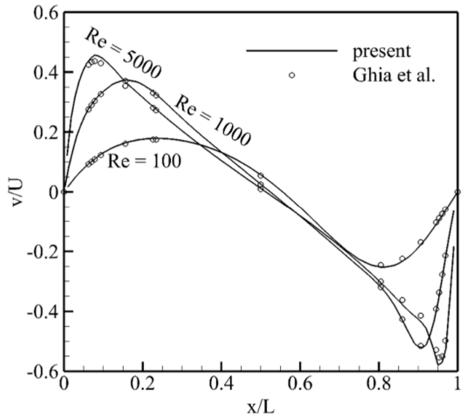


b) v-component velocity at y/L = 0.5

Figure 8. Comparison of the velocity profiles of present code based on AMR-FEM and previous results

### 3.2. 2D flow around a circular cylinder

The second benchmark problem is 2D flow through the cylinder. The schematic and the primary grid are shown in Fig. 9. The uniform velocity is set at the inlet, the non-slip condition is set at the cylinder, and the far-field is set at the bottom and the top. For the outlet, we use the convective outflow boundary condition proposed by Choi H.G [6]. Domain with length and width are set to 100D (H = 10m), the Reynolds number defined by the cylinder diameter D and the uniform velocity at the inlet $U_\infty$: $Re = \rho U_\infty L/\mu$. In this work, we simulate with Re = 40 and Re = 100 to get a steady flow and a vortex shedding flow, respectively.

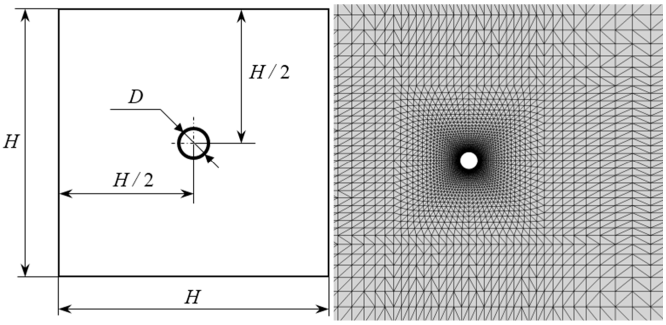


a) b)

Figure 9. The schematic (a) and the basic grid (b)

The solution is obtained in the final mesh, which is constructed based on the magnitude of the vorticity vector. Fig. 10 shows the final mesh and the vorticity field. This mesh will be fixed in the steady case (Re = 40) when the flow is stable (Fig. 10a). The final mesh is updated over time for the vortex shedding flow (Re = 100) (Fig. 10b).

Table 2 and Table 3 show the quantitative comparison of the present work and previous works. The results agree well with the others in the literature. The difference of present results with other recent results is less than 2% [14, 15]. The results from Martinez et al. are quite different from the others, maybe because of the low grid resolution at that time. In the case of Re = 100, the vortex shedding is appeared behind the cylinder (Fig 10.b) with a frequency f (also frequency of the lift force). Therefore, the Strouhal number (St) is a dimensionless number describing oscillating flow mechanisms and defined by:

$$St = \frac{f.D}{U_\infty} \tag{14}$$

Table 2. Comparison of the drag force coefficient ($C_d$)

| Re | Martinez et al. [13] | M. Braza et al. [14] | Park et al. [15] | Present work |
|---|---|---|---|---|
| 40 | 1.3 | 1.5 | 1.51 | 1.49 |
| 100 | 1.1 | 1.3 | 1.33 | 1.31 |

Table 3. Comparison of the Strouhal number (St) at the Re =100

| Martinez et al. [13] | Rahman et al. [16] | Park et al. [15] | Choi et al. [6] | Present work |
|---|---|---|---|---|
| 0.160 | 0.164 | 0.164 | 0.164 | 0.164 |

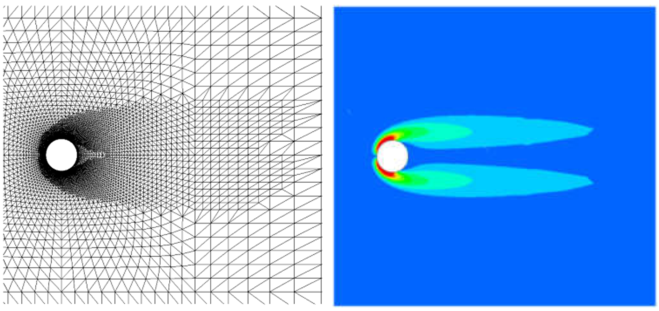

a) Re = 40

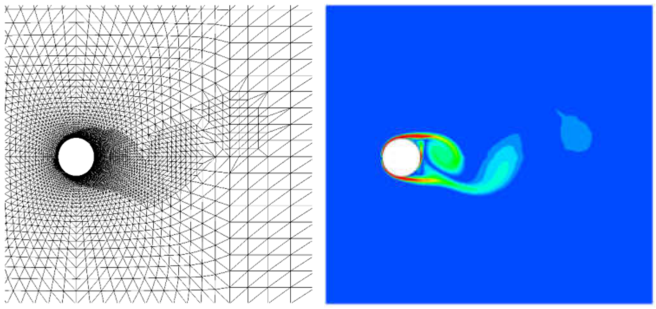

b) Re = 100 ( $tU_\infty$ / D = 101 )

Figure 10. Vorticity magnitude contour and its corresponding mesh

Lastly, Table 4 shows the CPU time comparison for the different types of a grid: Grid obtained by using AMR technique and the first full subdivision corresponding with their information of grid (for the case in Fig. 10b). It is confirmed that using the AMR technique can reduce more than three times for computational simulation.

Table 4. Comparison of CPU time

| Grid | First full subdivision | AMR Grid |
|---|---|---|
| No. nodes | 183,635 | 57,536 |
| CPU time | 15.12 s | 4.64 s |

## 4. CONCLUSION

This paper combines the finite element method (FEM) with an adaptive mesh refinement (AMR) technique on an unstructured grid to solve the Navier-Stokes equation for unsteady flow. A triangle P1P1 element was used to discrete the domain, and the projection three-step was adopted for solving the incompressible Navier-Stokes equation. In each time step, all elements' vorticity field magnitudes were obtained and employed as the indicator function for the element subdivision of the AMR technique. The two benchmarks have validated the method in a 2D unsteady fluid flow. The results confirmed that the present method with the AMR technique proposes an accurate solution compared to the excellent grid. The CPU time for the AMR process was short compared to the total computational time, and the FEM-AMR code can significantly reduce the CPU time, and it is a powerful approach for simulation of the large-scale problem. The extension of the 3D problem is straightforward and will be reported in future work.

## REFERENCES

[1]. J. Peraire, M. Vahdati, K. Morgan, O.C. Zienkiewicz, 1987. *Adaptive remeshing for compressible flow computations*. Journal of Computational physics, 72(2), 449-466.

[2]. M.J. Berger, J. Oliger, 1984. *Adaptive mesh refinement for hyperbolic partial differential equations*. Journal of Computational Physics, 53(3), 484-512.

[3]. X. Zhao, X. Hu, W. Cai, G.E. Karniadakis, 2017. *Adaptive finite element method for fractional differential equations using hierarchical matrices*. Computer Methods in Applied Mechanics and Engineering, 325, 56-76.

[4]. Frank Ethridge, Leslie Greengard, 2001. *A new fast-multipole accelerated Poisson solver in two dimensions*. SIAM Journal on Scientific Computing, 23.3, 741-760.

[5]. S.T. Ha, H.G. Choi, 2020. *Investigation on the effect of density ratio on the convergence behavior of the partitioned method for fluid-structure interaction simulation*. J. Fluids Struct, 96, 103050.

[6]. H.G. Choi, J.Y. Yoo, 1997. *A fractional four-step finite element formulation of the unsteady incompressible Navier-Stokes equations using SUPG and linear equal-order element methods*. Computer Methods in Applied Mechanics and Engineering, 143.3-4, 333-348.

[7]. L.C. Ngo, H.G. Choi, 2017. *A multi-level adaptive mesh refinement method for level set simulations of multiphase flow on unstructured meshes*. International Journal for Numerical Methods in Engineering, 110.10, 947-971.

[8]. S.Ø. Wille, 1996. *The prolonged adaptive multigrid method for finite element Navier-Stokes equations*. Computer methods in applied mechanics and engineering, 138(1-4), 227-271.

[9]. Stéphane Popinet, Gerris, 2003. *A tree-based adaptive solver for the incompressible Euler equations in complex geometries*. Journal of Computational Physics, 190.2, 572-600.

[10]. Y.S. Nam, H.G. Choi, J.Y. Yoo, 2002. *AILU preconditioning for the finite element formulation of the incompressible Navier–Stokes equations*. Computer methods in applied mechanics and engineering, 191.39-40, 4323-4339.

[11]. S.T. Ha, H.G. Choi, 2019. *Performance comparison of interpolation operators of the multigrid method based on a distance weighted and area (volume) intersection approaches.* Part II: Finite element discretization, Journal of Mechanical Science and Technology, 33.7, 3323-3331.

[12]. U. Ghia, K.N. Ghia, C.T. Shin, 1982. *High-Re solutions for incompressible flow using the Navier-Stokes equations and a multigrid method*. Journal of Computational Physics, 48, 387-411.

[13]. G. Martinez, H. Ha Minh, 1978. *Numerical methods in laminar and turbulent flow*. Proceedings of the First International Conference, University College of Swansea, Swansea, Wales.

[14]. M. Braza, P. Chassaing, H. Ha Minh, 1986. *Numerical study and physical analysis of the pressure and velocity fields in the near wake of a circular cylinder*. Journal of fluid mechanics, 165, 79-130

[15]. J. Park, K. Kwon, H. Choi, 1998. *Numerical solutions of flow past a circular cylinder at Reynolds numbers up to 160*. KSME International Journal, 12 (6), 1200–1205.

[16]. Rahman, Md Mahbubar, Md Mashud Karim, Md Abdul Alim, 2007. *Numerical investigation of unsteady flow past a circular cylinder using 2D finite volume method*. Journal of Naval Architecture and Marine Engineering, 4.1, 27-42.

**THÔNG TIN TÁC GIẢ**

**Nguyễn Mạnh Hùng[1], Hà Trường Sang[1], Lê Văn Dưỡng[2]**

[1]Khoa Cơ khí, Học viện Kỹ thuật Quân sự

[2]Khoa Động lực, Học viện Kỹ thuật Quân sự